Appl. Math. Mech. -Engl. Ed., **43**(8), 1289–1306 (2022)

APPLIED MATHEMATICS AND MECHANICS (ENGLISH EDITION)

https://doi.org/10.1007/s10483-022-2886-5

Electrokinetic flow and energy conversion in a curved microtube*

Zhaodong DING, Kai TIAN, Yongjun JIAN†

School of Mathematical Science, Inner Mongolia University, Hohhot 010021, China

(Received Dec. 27, 2021 / Revised May 19, 2022)

Abstract Curved channels are ubiquitous in microfluidic systems. The pressure-driven electrokinetic flow and energy conversion in a curved microtube are investigated analytically by using a perturbation analysis method under the assumptions of the small curvature ratio and the Reynolds number. The results indicate that the curvature of the microtube leads to a skewed pattern in the distribution of the electrical double layer (EDL) potential. The EDL potential at the outer side of the bend is larger than that at the inner side of the bend. The curvature shows an inhibitory effect on the magnitude of the streaming potential field induced by the pressure-driven flow. Since the spanwise pressure gradient is dominant over the inertial force, the resulting axial velocity profile is skewed into the inner region of the curved channel. Furthermore, the flow rate in a curved microtube could be larger than that in a straight one with the same pressure gradient and shape of cross section. The asymptotic solutions of the axial velocity and flow rate in the absence of the electrokinetic effect are in agreement with the classical results for low Reynolds number flows. Remarkably, the curved geometry could be beneficial to improving the electrokinetic energy conversion (EKEC) efficiency.

Key words electrokinetic flow, streaming potential, electrokinetic energy conversion (EKEC), perturbation analysis method, curved microchannel

Chinese Library Classification O357.1
2010 Mathematics Subject Classification 76D05, 76V05

1 Introduction

Manipulating flows at micro-scales are important for many scientific disciplines and industrial applications[1]. Nowadays, microfluidic devices have been widely used in biochemical and biomedical processes, fuel cells, physical particle separation, and heat exchange[2–3]. Curved channel appears to be ubiquitous for these systems. On the one hand, it provides a convenient scheme for increasing the channel length per unit chip area in the direction of net flow. On the other hand, the design of curved channels can be used to enhance micro-mixing[4] and reaction in continuous flow reactors[5].

∗ Citation: DING, Z. D., TIAN, K., and JIAN, Y. J. Electrokinetic flow and energy conversion in a curved microtube. *Applied Mathematics and Mechanics* (*English Edition*), **43**(8), 1289–1306 (2022) https://doi.org/10.1007/s10483-022-2886-5

† Corresponding author, E-mail: jianyj@imu.edu.cn

Project supported by the National Natural Science Foundation of China (Nos. 11902165 and 11772162), the Natural Science Foundation of Inner Mongolia Autonomous Region of China (No. 2019BS01004), and the Inner Mongolia Grassland Talent of China (No. 12000-12102408)

Fluid flow in a curved pipe is a classical problem in fluid dynamics[6–7]. Dean[8–9] was the first to develop an analytical solution for fully developed laminar flow in a curved tube of circular cross section under the condition of small curvature ratio, $\delta = a/R$, where a and R are the radii of the tube and the coil, respectively. The series solution developed by Dean only depends on a single non-dimensional parameter, the Dean number, which is essentially a product of the square of a Reynolds number and the curvature ratio δ. The system exhibits a secondary flow pattern of two counter-rotating vortices (Dean vortices). The axial velocity profile is not axisymmetric. In addition, the flow rate in a curved channel is lower than that in a straight channel for a given axial pressure gradient with a moderate Reynolds number.

In microflows, surface effects become the dominant factor due to the relatively large surface area to fluid volume ratio[10]. When a solid surface is in contact with a polarizable electrolyte solution, the solid surface may attain a net positive or negative charge due to ion adsorption from the liquid molecules adjacent to it. This leads to the presence of the electrical potential at the surface, which is well known as the wall zeta potential. Due to the electrostatic interactions, the migration of ions naturally arises between the dielectric walls and the polar fluid. Here, the charged wall of the microchannel attracts counter-ions in the liquid forming the so-called electrical double layer (EDL). The characteristic thickness of the EDL is commonly known as the Debye length[11].

Electrokinetic phenomena induced by the EDL play an important role in microfluidic transport[12]. Application of an electric field along a fluidic conduit with surface charge induces movement of mobile ions in the EDL, and viscous forces in the solution drag adjacent fluid layers along the same direction, resulting in the electroosmotic flow (EOF). This is named as the "pumping mode"[13]. When an electrolyte solution is driven by an applied pressure gradient through a microchannel, the movement of net charges in the EDL causes an electric current (known as the streaming current). Furthermore, the accumulation of charges at the channel downstream creates an induced electrical potential difference (called the streaming potential) between the ends of the microchannel, which is the so-called "generation mode"[13]. The establishment of the streaming current and streaming potential in microchannels represents a means of the converting hydrostatic energy into the electrical power[14]. Experimental and theoretical studies demonstrated that the streaming current can provide a simple and effective means of transferring the mechanical energy of the pressure-driven transport and chemical energy of the EDL to electrical power of the streaming current[15–20]. The conversion between electrical energy and mechanical energy in microchannels via the electrokinetic effect refers to the electrokinetic energy conversion (EKEC).

We noticed that previous studies were almost confined to the analysis of electrokinetic phenomena in straight channels. However, curved channels are ubiquitous for microfluidic systems. Despite the important applications, the electrokinetic flow in curved microchannels has received much less attention in the literature. Luo[21] applied a numerical approach to investigate transient electroosmotic flow in a curved rectangular channel in which the fluid is driven by an external direct current (DC) or alternating current (AC) electric field. Using a finite volume scheme, Yun et al.[22] simulated the pressure-driven electrokinetic flow in curved rectangular channels, and recognized the skewed pattern in a streamwise velocity for the case of a low Reynolds number.

In curved microchannels, it is difficult to analytically solve a coupled set of partial differential equations, i.e., Navier-Stokes (for incompressible fluid flow) and Poisson-Boltzmann (for EDL potential). To the best of the authors' knowledge, the present research of the electrokinetic flows in curved pipes mainly relies on numerical simulations, and little progress has been made analytically. In this study, we provide an analytical investigation of the fully developed electrokinetic flow, based on a perturbation analysis, in a curved microtube under the condition of small curvature ratio. Using the analytical solutions, we can explore the effects of the curvature of the curved microtube on the velocity, flow rate, EDL potential, streaming potential, and EKEC, and evaluate the performance characteristics.

2 Basic equations

To begin with, we consider a pressure-driven and steady-state microfluidic transport through a curved microtube with a uniform curvature. The geometry of the problem and the attached toroidal coordinate system (r, θ, ϕ) are sketched in Fig. 1, where a is the radius of the circular cross section of the channel, C is located at the centre of the section of the channel, the centreline of the tube is assumed to lie on the arc of a circle of radius R (e.g., $R = \overline{OC}$ in Fig. 1), xy-plane coincides with the centre plane of the channel (i.e., the plane containing the centreline), and the channel curves about the z-axis. The transformation from the rectangular coordinates (x, y, z) to the toroidal coordinate system (r, θ, ϕ) is

$$x = (R + r\cos\theta)\cos\phi, \quad y = (R + r\cos\theta)\sin\phi, \quad z = r\sin\theta. \tag{1}$$

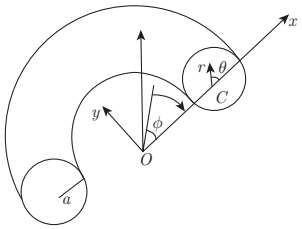

Fig. 1 The channel geometry and related coordinate systems

We introduce the following assumptions: (i) the channel has a small curvature ratio a/R; (ii) the electrokinetic flow in a curved microchannel is a low Reynolds number flow. The assumption (i) facilitates the development of an asymptotic solution in mathematics. Generally, for the electrokinetic flow in microchannels, both the dimension of the channel and the velocity of the fluid are small, and thus the assumption (ii) is reasonable. In addition, the characteristic length of the channel is considered to be micro-scale, while the thickness of the EDL is generally in nano-level (several to hundreds of nanometers). Therefore, the thin EDL approximation can also be used reasonably.

2.1 Distribution of the electrostatic potential in a curved microtube

In a microchannel filled with an electrolyte solution with a uniform dielectric constant ε and viscosity μ, when the liquid comes into contact with the solid wall, interfacial charges are induced. The charges cause the free ions in the liquid to rearrange to form a thin region (i.e., the EDL) with non-zero net charge density, in which an electrical potential field (denoted by $\widetilde{\psi}_e$) is established. On the other hand, when driven by an applied pressure gradient through the microchannel, the flow with net charges will lead to the presence of streaming potential, denoted by $\widetilde{\psi}_{\rm s}$. Therefore, the overall electrical potential $\widetilde{\Psi}$ is composed by both ψ_e and $\widetilde{\psi}_{\rm s}$, i.e., $\widetilde{\Psi} = \widetilde{\psi}_e + \widetilde{\psi}_{\rm s}$. According to the electrostatics theory, the potential $\widetilde{\Psi}$ satisfies the Poisson equation, i.e.,

$$\nabla^2\widetilde{\Psi} = -\frac{\widetilde{\rho}_e}{\varepsilon}, \tag{2}$$

where $\widetilde{\rho}_e$ is the net electric charge density.

In a straight microtube with circular section, the potential $\widetilde{\psi}_e$ is only a function of r. However, in a slightly curved circular microtube, the potential $\widetilde{\psi}_e$ is also θ-dependent due to the breaking of axisymmetry, i.e., $\widetilde{\psi}_e = \widetilde{\psi}_e(r, \theta)$. Furthermore, for the case of thin EDL, it is acceptable that the spanwise dependence of the flow-induced streaming potential $\widetilde{\psi}_{\rm s}$ is much smaller than its streamwise axial dependence[22]. Thus, $\widetilde{\psi}_{\rm s} = \widetilde{\psi}_{\rm s}(\phi)$ can be applied. With these assumptions, Eq. (2) readily reduces to

$$\nabla^2\widetilde{\psi}_e(r, \theta) = -\frac{\widetilde{\rho}_e}{\varepsilon}, \tag{3}$$

$$\nabla^2\widetilde{\psi}_{\rm s}(\phi)=0. \tag{4}$$

The net charge density $\widetilde{\rho}_e$ can be written, by assuming a symmetric electrolyte ($z_+=-z_-=z_{\rm v}$), as

$$\widetilde{\rho}_e=e(z_+n_++z_-n_-)=e\,z_{\rm v}(n_+-n_-), \tag{5}$$

where e is the electron charge, $z_{\rm v}$ is the valence, and n_+ and n_- are the respective ionic number densities of the electrolyte cations and anions, respectively, being expressed through the Boltzmann distribution

$$n_\pm=n_0\exp\Big(\mp\frac{z_{\rm v}e\widetilde{\psi}_e}{k_{\rm B}T}\Big) \tag{6}$$

with the ion density n_0 of bulk liquid, the Boltzmann constant $k_{\rm B}$, and the absolute temperature T. Note that the Boltzmann equation (6) is valid when the EDL of two adjacent walls do not overlap.

Substitution of Eqs. (5) and (6) into Eq. (3) yields the celebrated Poisson-Boltzmann equation

$$\nabla^2\widetilde{\psi}_e=\frac{2n_0z_{\rm v}e}{\varepsilon}\sinh\Big(\frac{z_{\rm v}\,e\widetilde{\psi}_e}{k_{\rm B}T}\Big). \tag{7}$$

In the curvilinear coordinate system, Eq. (7) can be expressed as

$$\begin{aligned}&\frac{\partial^2\widetilde{\psi}_e}{\partial r^2}+\frac{1}{r}\frac{\partial\widetilde{\psi}_e}{\partial r}+\frac{\cos\theta}{R+r\cos\theta}\frac{\partial\widetilde{\psi}_e}{\partial r}+\frac{1}{r^2}\frac{\partial^2\widetilde{\psi}_e}{\partial\theta^2}-\frac{\sin\theta}{r(R+r\cos\theta)}\frac{\partial\widetilde{\psi}_e}{\partial\theta}\\&=\frac{2n_0z_{\rm v}e}{\varepsilon}\sinh\Big(\frac{z_{\rm v}e\widetilde{\psi}_e}{k_{\rm B}T}\Big),\end{aligned} \tag{8}$$

subject to the following boundary condition:

$$\widetilde{\psi}_e(r,\theta)\Big|_{r=a}=\widetilde{\varphi}. \tag{9}$$

Here, $\widetilde{\varphi}$ is the wall zeta potential.

Equation (4), in the coordinate system, can be expressed as

$$\frac{{\rm d}^2\widetilde{\psi}_{\rm s}}{{\rm d}\phi^2}=0. \tag{10}$$

This means that ${\rm d}\widetilde{\psi}_{\rm s}/{\rm d}\phi$ is a constant. Let

$$\widetilde{E}_{\rm s}=-\frac{1}{R}\frac{{\rm d}\widetilde{\psi}_{\rm s}}{{\rm d}\phi} \tag{11}$$

denote the magnitude of the electric field strength related to the streaming potential along the centerline of the tube (i.e., $r=0$).

2.2 Governing equations of fluid motion

The steady-state fluid flow is governed by the continuity and momentum equations,

$$\nabla\cdot\widetilde{\boldsymbol{V}}=0, \tag{12}$$

$$\rho(\widetilde{\boldsymbol{V}}\cdot\nabla)\widetilde{\boldsymbol{V}}=-\nabla p+\mu\nabla^2\widetilde{\boldsymbol{V}}+\boldsymbol{F}, \tag{13}$$

where $\widetilde{\boldsymbol{V}}=(\widetilde{v}_r,\widetilde{v}_\theta,\widetilde{v}_\phi)$ is the velocity vector, ρ is the fluid density, p is the pressure, $\boldsymbol{F}=\widetilde{\rho}_e\widetilde{\boldsymbol{E}}$ is the body force as a result of the action of the electric field on the free ions within the EDL, $\widetilde{\rho}_e$ is given by Eq. (5), and the electric field $\widetilde{\boldsymbol{E}}$ satisfies

$$\widetilde{\boldsymbol{E}}=-\nabla\widetilde{\Psi}=-\Big(\frac{\partial\widetilde{\Psi}}{\partial r},\ \frac{1}{r}\frac{\partial\widetilde{\Psi}}{\partial\theta},\ \frac{1}{R+r\cos\theta}\frac{\partial\widetilde{\Psi}}{\partial\phi}\Big)^{\rm T}. \tag{14}$$

Under the assumption of the low Reynolds number or creeping flow, the inertial term on the left side of Eq. (13) can be neglected. Furthermore, the lateral parts of velocity components

can be omitted in comparison with the order of magnitude of streamwise velocity (i.e., $\widetilde{v_r} = \widetilde{v}_\theta = 0$). In fact, by numerical simulation of steady electrokinetic flow in a curved rectangular microchannel, Yun et al.[22] has found that the magnitude of the spanwise velocity is smaller in the order of 10^{-5}–10^{-7} than that of the axial velocity. This is also consistent with the result demonstrated experimentally by Yamaguchi et al.[23] in the case of a low Reynolds number. In addition, since the flow is fully developed, the axial velocity component $\widetilde{v}_\phi = \widetilde{v}_\phi(r,\theta)$ is independent of ϕ. Thus, Eq. (12) is satisfied automatically, and only the ϕ-momentum equation should be solved, which in the toroidal coordinate system can be expressed as

$$\mu\Big(\Big(\frac{\partial}{\partial r}+\frac{1}{r}\Big)\Big(\frac{\partial\widetilde{v}_\phi}{\partial r}+\frac{\widetilde{v}_\phi\cos\theta}{R+r\cos\theta}\Big)+\frac{1}{r}\frac{\partial}{\partial\theta}\Big(\frac{1}{r}\frac{\partial\widetilde{v}_\phi}{\partial\theta}-\frac{\widetilde{v_\phi}\sin\theta}{R+r\cos\theta}\Big)\Big) - \frac{1}{R+r\cos\theta}\frac{\partial p}{\partial\phi}-\frac{\widetilde{\rho}_e}{R+r\cos\theta}\frac{\mathrm{d}\widetilde{\psi}_\mathrm{s}}{\mathrm{d}\phi}=0 \tag{15}$$

with the no-slip boundary condition

$$\widetilde{v}_\phi(r,\theta)|_{r=a}=0. \tag{16}$$

So far, the equations governing the distributions of the EDL potential and the axial velocity have been established by Eqs. (8) and (15), with the corresponding boundary conditions (9) and (16). Then, we introduce the following dimensionless quantities:

$$\begin{cases} r'=\dfrac{r}{a}, \quad \psi_e=\dfrac{z_\mathrm{v}e\widetilde{\psi}_e}{k_\mathrm{B}T}, \quad k=\dfrac{a}{\lambda}, \quad \varphi=\dfrac{z_\mathrm{v}e\widetilde{\varphi}}{k_\mathrm{B}T}, \\ \rho_e=\dfrac{z_\mathrm{v}ea^2}{\varepsilon k_\mathrm{B}T}\widetilde{\rho}_e, \quad u=\dfrac{\widetilde{v}_\phi}{u_{p,0}}, \quad u_r=\dfrac{u_{e,0}}{u_{p,0}}, \quad E_\mathrm{s}=\dfrac{\widetilde{E}_\mathrm{s}}{E_0}, \end{cases} \tag{17}$$

where k is the inverse of the dimensionless Debye length (also known as the electrokinetic width), $\lambda=\sqrt{\frac{\varepsilon k_\mathrm{B}T}{2n_0e^2z_\mathrm{v}^2}}$ is the Debye length, $u_{p,0}=-\frac{a^2}{\mu R}\frac{\partial p}{\partial\phi}$ is the pressure-driven velocity scale, $u_{e,0}=-\frac{\varepsilon k_\mathrm{B}T}{z_\mathrm{v}e}\frac{E_0}{\mu}$ is the electroosmotic velocity scale, u_r denotes the ratio of the electro-osmotic velocity to the pressure-driven characteristic velocity, and E_0 is the characteristic electric field strength.

Assuming that the wall zeta potentials $\widetilde{\varphi}$ is small enough, the Debye-Hückel linearization approximation can be applied on the right hand side of Eq. (8). The dimensionless forms of Eqs. (8) and (15) as well as the boundary conditions (9) and (16) can be written as

$$\frac{\partial^2\psi_e}{\partial r^2}+\frac{1}{r}\frac{\partial\psi_e}{\partial r}+\frac{\delta\cos\theta}{1+\delta r\cos\theta}\frac{\partial\psi_e}{\partial r}+\frac{1}{r^2}\frac{\partial^2\psi_e}{\partial\theta^2}-\frac{\delta\sin\theta}{r(1+\delta r\cos\theta)}\frac{\partial\psi_e}{\partial\theta}=k^2\psi_e, \tag{18}$$

$$\Big(\Big(\frac{\partial}{\partial r}+\frac{1}{r}\Big)\Big(\frac{\partial u}{\partial r}+\frac{u\delta\cos\theta}{1+\delta r\cos\theta}\Big)+\frac{1}{r}\frac{\partial}{\partial\theta}\Big(\frac{1}{r}\frac{\partial u}{\partial\theta}-\frac{u\delta\sin\theta}{1+\delta r\cos\theta}\Big)\Big) + \frac{1}{1+\delta r\cos\theta}-\frac{u_rE_\mathrm{s}}{1+\delta r\cos\theta}\rho_e=0, \tag{19}$$

$$\psi_e(r,\theta)|_{r=1}=\varphi, \tag{20}$$

$$u(r,\theta)|_{r=1}=0. \tag{21}$$

Note that in the above equations, we have simply used r instead of r' in the case of no confusion, $\delta=a/r$ denotes the curvature ratio, which is assumed to be small. Using these dimensionless variables and Debye-Hückel linearization, Eqs. (5) and (6) reduce to

$$\rho_e=-k^2\psi_e, \tag{22}$$

which can be used in Eq. (19).

3 Perturbation solutions

In the governing equations (18) and (19), the parameter δ reflects the characteristic of a curved microtube. When δ vanishes, these equations will reduce to those classical equations describing electrokinetic flows in straight channels. The parameter δ is not only a measure of the effect of geometry, but also plays a major role in curved channel flows. For small values of δ, the solution can be expressed by a regular perturbation expansion in δ for relevant variables as

$$\begin{cases} \psi_e = \psi_0(r) + \delta\psi_1(r,\theta) + \delta^2\psi_2(r,\theta) + O(\delta^3), \\ u = u_0(r) + \delta u_1(r,\theta) + \delta^2 u_2(r,\theta) + O(\delta^3), \\ E_{\rm s} = E_{\rm s,0} + \delta E_{\rm s,1} + \delta^2 E_{\rm s,2} + O(\delta^3). \end{cases} \tag{23}$$

Here, we point out that due to the influence of curvature, the distribution of streaming potential $E_{\rm s}$, caused by the application of an external pressure-driven transport, will deviate from that of a nominally straight channel, and thus it should be also expressed in the form of power series in δ.

Substitution of Eq. (23) into Eqs. (18) and (19) yields a series of differential equations for every powers of δ as follows:

$$\delta^0: \ \frac{{\rm d}^2\psi_0}{{\rm d}r^2} + \frac{1}{r}\frac{{\rm d}\psi_0}{{\rm d}r} = k^2\psi_0, \tag{24}$$

$$1 + \Big(\frac{\rm d}{{\rm d}r} + \frac{1}{r}\Big)\frac{{\rm d}u_0}{{\rm d}r} + k^2 u_r E_{\rm s,0}\psi_0 = 0, \tag{25}$$

$$\delta^1: \ \frac{\partial^2\psi_1}{\partial r^2} + \frac{1}{r}\frac{\partial\psi_1}{\partial r} + \frac{1}{r^2}\frac{\partial^2\psi_1}{\partial\theta^2} + \cos\theta\frac{{\rm d}\psi_0}{{\rm d}r} = k^2\psi_1, \tag{26}$$

$$\begin{aligned} &\Big(\frac{\partial}{\partial r} + \frac{1}{r}\Big)\Big(\frac{\partial u_1}{\partial r} + u_0\cos\theta\Big) + \frac{1}{r}\frac{\partial}{\partial\theta}\Big(\frac{1}{r}\frac{\partial u_1}{\partial\theta} - u_0\sin\theta\Big) + k^2 u_r \\ &\times (E_{\rm s,0}\psi_1 + E_{\rm s,1}\psi_0 - E_{\rm s,0}\psi_0 r\cos\theta) = r\cos\theta, \end{aligned} \tag{27}$$

$$\delta^2: \ \frac{\partial^2\psi_2}{\partial r^2} + \frac{1}{r}\frac{\partial\psi_2}{\partial r} + \frac{1}{r^2}\frac{\partial^2\psi_2}{\partial\theta^2} + \cos\theta\frac{\partial\psi_1}{\partial r} - \frac{\sin\theta}{r}\frac{\partial\psi_1}{\partial r} - r\cos^2\theta\frac{{\rm d}\psi_0}{{\rm d}r} = k^2\psi_2, \tag{28}$$

$$\begin{aligned} &\Big(\frac{\partial}{\partial r} + \frac{1}{r}\Big)\Big(\frac{\partial u_2}{\partial r} + u_1\cos\theta - r u_0\cos^2\theta\Big) + \frac{1}{r^2}\frac{\partial^2 u_2}{\partial\theta^2} \\ &- \frac{1}{r}\frac{\partial}{\partial\theta}(u_1\sin\theta - r u_0\cos\theta\sin\theta) + k^2 u_r(E_{\rm s,0}\psi_2 + E_{\rm s,1}\psi_1 - E_{\rm s,2}\psi_0 - r\cos\theta \\ &\times (E_{\rm s,0}\psi_1 + E_{\rm s,1}\psi_0) + r^2\cos^2\theta E_{\rm s,0}\psi_0) = -r^2\cos^2\theta. \end{aligned} \tag{29}$$

The solutions to Eqs. (24)–(29) constrained by the corresponding boundary conditions will be developed and discussed in the following. First, it can be recognized that Eqs. (24) and (25) correspond to the fully developed and steady electrokinetic flow in a straight microchannel with circular cross section. Both the zeroth-order EDL potential and the zeroth-order axial velocity are axisymmetric, and thus they are independent of θ. That is the reason that in the regular perturbation expansion (23), we have assumed ψ_0 and u_0 as a function of r only. With the corresponding boundary conditions

$$\psi_0(1) = \varphi, \quad u_0(1) = 0, \tag{30}$$

the solution to the zeroth-order equations in δ is straightforward and well documented, i.e.,

$$\psi_0 = \varphi\frac{{\rm I}_0(kr)}{{\rm I}_0(k)}, \quad u_0 = \frac{1-r^2}{4} + \varphi u_r E_{\rm s,0}\Big(1 - \frac{{\rm I}_0(kr)}{{\rm I}_0(k)}\Big), \tag{31}$$

where ${\rm I}_0$ is the zeroth-order modified Bessel function of the first kind.

3.1 First- and second-order solutions for EDL potential and velocity

In order to investigate the curvature effect on the electrokinetic flow, it is necessary to solve the high-order equations in δ, i.e., Eqs. (26)–(29), with the corresponding boundary conditions

$$\psi_1(r,\theta)|_{r=1}=0, \quad u_1(r,\theta)|_{r=1}=0, \tag{32}$$

$$\psi_2(r,\theta)|_{r=1}=0, \quad u_2(r,\theta)|_{r=1}=0. \tag{33}$$

To facilitate this, based upon the form of Eq. (26), ψ_1 can be assumed to take the form

$$\psi_1(r,\theta)=f_1(r)\cos\theta. \tag{34}$$

Substitution of Eq. (34) into Eq. (26) yields a differential equation with respect to f_1

$$r^2\frac{\mathrm{d}^2 f_1}{\mathrm{d}r^2}+r\frac{\mathrm{d}f_1}{\mathrm{d}r}-(1+k^2r^2)f_1=-\frac{kr^2\mathrm{I}_1(kr)}{\mathrm{I}_0(k)}\varphi \tag{35}$$

with the related boundary condition

$$f_1(1)=0. \tag{36}$$

By means of the eigenfunction expansion, f_1 can be expressed as

$$f_1(r)=\sum_{n=1}^{\infty}A_n\mathrm{J}_1(\mu_{n,1}r). \tag{37}$$

Here and henceforth, J_v denotes the vth order Bessel function of the first kind, and $\mu_{n,v}$ is the nth positive root of $\mathrm{J}_v(r)=0$. By substituting Eq. (37) into Eq. (35) and utilizing the orthogonality of $\mathrm{J}_1(\mu_{n,1}r)$ in the interval $[0,1]$, these coefficients A_n can be determined and finally the solution f_1 can be obtained as

$$f_1(r)=\sum_{n=1}^{\infty}\frac{2\varphi b_{n,1}}{(\mu_{n,1}^2+k^2)\mathrm{J}_0(\mu_{n,1})}\mathrm{J}_1(\mu_{n,1}r), \tag{38}$$

where

$$b_{n,1}=\frac{k}{\mathrm{I}_0(k)}\int_0^1 r\mathrm{I}_1(kr)\mathrm{J}_1(\mu_{n,1}r)\mathrm{d}r. \tag{39}$$

Similar to the process of solving Eq. (26), the solution to Eq. (27) can be assumed, based on Eqs. (31) and (34), to take the form

$$u_1(r,\theta)=U_1(r)\cos\theta+U_2(r), \tag{40}$$

which is subject to the boundary condition (32). The functions U_1 and U_2 can be obtained as follows:

$$\begin{aligned}U_1(r)=&\frac{3r(r^2-1)}{16}+\frac{\varphi u_r E_{\mathrm{s},0}}{k\mathrm{I}_0(k)}(\mathrm{I}_1(kr)-r\mathrm{I}_1(k)+rk\mathrm{I}_2(kr)-kr\mathrm{I}_2(k))\\&+\sum_{n=1}^{\infty}\frac{2\varphi u_r E_{\mathrm{s},0}k^2 b_{n,1}}{\mu_{n,1}^2(\mu_{n,1}^2+k^2)\mathrm{J}_0^2(\mu_{n,1})}\mathrm{J}_1(\mu_{n,1}r),\end{aligned} \tag{41}$$

$$U_2(r)=\varphi u_r E_{\mathrm{s},1}\Big(1-\frac{\mathrm{I}_0(kr)}{\mathrm{I}_0(k)}\Big). \tag{42}$$

When the streaming potential vanishes, the first-order velocity reduces to

$$u_1^*(r,\theta)=\frac{3r(r^2-1)}{16}\cos\theta. \tag{43}$$

The second-order problem, i.e., Eqs. (28) and (29), is more complicated. Its solution can be expressed as

$$\begin{cases}\psi_2(r,\theta)=g(r)+h(r)\cos(2\theta),\\ u_2(r,\theta)=V_1(r)+V_2(r)\cos\theta+V_3(r)\cos(2\theta).\end{cases} \tag{44}$$

Based on Eqs. (31), (37), and (38), and the boundary condition (33), the functions g and h can be obtained as follows:

$$\begin{cases} g(r) = -\displaystyle\sum_{n=1}^{\infty} \frac{\varphi b_{n,0}}{(\mu_{n,0}^2+k^2)\mathrm{J}_1^2(\mu_{n,0})}\mathrm{J}_0(\mu_{n,0}r) \\ \qquad\quad + \displaystyle\sum_{n=1}^{\infty} \frac{\varphi \mu_{n,1} b_{n,1}}{(\mu_{n,1}^2+k^2)^2\mathrm{J}_2^2(\mu_{n,1})}\Big(\mathrm{J}_0(\mu_{n,1}r) - \frac{\mathrm{J}_0(\mu_{n,1})}{\mathrm{I}_0(k)}\mathrm{I}_0(kr)\Big), \\ h(r) = -\displaystyle\sum_{n=1}^{\infty} \frac{\varphi b_{n,2}}{(\mu_{n,2}^2+k^2)\mathrm{J}_1^2(\mu_{n,2})}\mathrm{J}_2(\mu_{n,2}r) \\ \qquad\quad + \displaystyle\sum_{n=1}^{\infty} \frac{\varphi \mu_{n,1} b_{n,1}}{(\mu_{n,1}^2+k^2)^2\mathrm{J}_2^2(\mu_{n,1})}\Big(\frac{\mathrm{J}_2(\mu_{n,1})}{\mathrm{I}_2(k)}\mathrm{I}_2(kr) - \mathrm{J}_2(\mu_{n,1}r)\Big), \end{cases} \tag{45}$$

where

$$b_{n,v} = \frac{k}{\mathrm{I}_0(k)}\int_0^1 r\mathrm{I}_1(kr)\mathrm{J}_v(\mu_{n,v}r)\mathrm{d}r, \quad v = 0, 1, 2. \tag{46}$$

The detailed expressions for V_1, V_2, and V_3 are sophisticated and not given here. When the influence of the streaming potential vanishes, the second-order velocity reduces to

$$u_2^*(r,\theta) = \frac{14r^2 - 3 - 11r^4}{128} + \frac{5r^2(1-r^2)}{64}\cos(2\theta). \tag{47}$$

Combining Eqs. (31), (34), (40), and (44), the approximate solutions of the EDL potential and the axial velocity up to second-order have been derived.

3.2 Calculation of the streaming potential

In order to obtain the streaming potential, we first consider the total ionic current through the channel section, which is expressed as

$$\widetilde{I}_{\mathrm{ionic}} = ez_{\mathrm{v}}\int_0^{2\pi}\mathrm{d}\theta\int_0^a (n_+\widetilde{v}_\phi^+ - n_-\widetilde{v}_\phi^-)r\mathrm{d}r. \tag{48}$$

Here, $\widetilde{v}_\phi^{\pm}$ refer to the axial velocities of the cations and anions, and they are a combination of the fluid advection velocity and the electromigrative velocity, i.e.,

$$\widetilde{v}_\phi^{\pm} = \widetilde{v}_\phi \pm \frac{R}{R + r\cos\theta}\frac{ez_{\mathrm{v}}\widetilde{E}_{\mathrm{s}}}{f}, \tag{49}$$

where f is the ionic friction coefficient (assumed to be identical for cations and anions). Note that in Eq. (49), there is an additional factor $R/(R + r\cos\theta)$ appearing in the traditional electromigrative velocity $ez_{\mathrm{v}}\widetilde{E}_{\mathrm{s}}/f$, due to the bending of the channel, and it is close to one when $R \gg r$.

By using Eqs. (6) and (49), and the dimensionless variables (17), and applying the Debye-Hückel linearization approximation, the total ionic current can be rewritten as

$$\widetilde{I}_{\mathrm{ionic}} = \widetilde{I}_{\mathrm{s}} + \widetilde{I}_{\mathrm{c}} = -2n_0ez_{\mathrm{v}}a^2u_{p,0}\Big(\int_0^{2\pi}\mathrm{d}\theta\int_0^1\psi_e u r\mathrm{d}r + Mu_rE_{\mathrm{s}}\int_0^{2\pi}\mathrm{d}\theta\int_0^1\frac{r\mathrm{d}r}{1+\delta\cos\theta}\Big), \tag{50}$$

where $\widetilde{I}_{\mathrm{s}}$ is streaming current, $\widetilde{I}_{\mathrm{c}}$ is conduction current, and $M = \frac{e^2z_{\mathrm{v}}^2\mu}{\varepsilon k_{\mathrm{B}}Tf}$ is a dimensionless parameter, determining the dimensionless conduction current, which is often interpreted as the inverse of the ionic Peclet number[24]. For pressure-driven transport, $\widetilde{I}_{\mathrm{ionic}}$ becomes identically zero at steady state; the corresponding value of E_{s} is known as the streaming potential field (customarily, E_{s} is also called the streaming potential). Thus, E_{s} can be obtained by solving the following equation:

$$-Mu_rE_{\mathrm{s}}\int_0^{2\pi}\mathrm{d}\theta\int_0^1\frac{r\mathrm{d}r}{1+\delta r\cos\theta} = \int_0^{2\pi}\mathrm{d}\theta\int_0^1\psi_e(r,\theta)u(r,\theta)r\mathrm{d}r. \tag{51}$$

Using the expansions (23) and collecting terms of equal powers of δ, we get a series of equations as follows:

$$\delta^0: \quad -\pi M u_r E_{\mathrm{s},0} = 2\pi \int_0^1 \psi_0(r) u_0(r) r \mathrm{d}r, \tag{52}$$

$$\delta^1: \quad -\pi M u_r E_{\mathrm{s},1} = 2\pi\varphi^2 u_r E_{\mathrm{s},1} \int_0^1 \frac{\mathrm{I}_0(kr)}{\mathrm{I}_0(k)}\Big(1 - \frac{\mathrm{I}_0(kr)}{\mathrm{I}_0(k)}\Big) r \mathrm{d}r, \tag{53}$$

$$\delta^2: \quad -\pi M u_r \Big(E_{\mathrm{s},2} + \frac{1}{4} E_{\mathrm{s},0}\Big) = 2\pi \int_0^1 (g(r)u_0(r) + \psi_0(r)V_1(r)) r \mathrm{d}r + 2\varphi\pi \times \sum_{n=1}^{\infty} \frac{b_{n,1}}{(\mu_{n,1}^2 + k^2)\mathrm{J}_0^2(\mu_{n,1})} \int_0^1 u_1(r) r \mathrm{J}_1(\mu_{n,1} r) \mathrm{d}r. \tag{54}$$

After substituting Eq. (31) into Eq. (52), the leading-order solution $O(\delta^0)$ yields

$$E_{\mathrm{s},0} = -\frac{\frac{\varphi}{2}\int_0^1 r(1-r^2)\frac{\mathrm{I}_0(kr)}{\mathrm{I}_0(k)}\mathrm{d}r}{u_r M + 2\varphi^2 u_r \int_0^1 \frac{\mathrm{I}_0(kr)}{\mathrm{I}_0(k)}\big(1 - \frac{\mathrm{I}_0(kr)}{\mathrm{I}_0(k)}\big) r \mathrm{d}r} = -\frac{\varphi \mathrm{I}_2(k)}{k^2 u_r \big(M\mathrm{I}_0(k) + \varphi^2\big(\frac{\mathrm{I}_1^2(k)}{\mathrm{I}_0(k)} - \mathrm{I}_2(k)\big)\big)}. \tag{55}$$

This is consistent with the streaming potential in straight channels for the pressure-driven transports[25]. Note that the zeroth-order streaming potential field has a sign opposite to the surface zeta potential φ, and it will trigger an electroosmotic transport that opposes the pressure-driven transport (see Eq. (31)). In order to make Eq. (53) hold, the first-order streaming potential $E_{\mathrm{s},1}$ must vanish. That means the curvature of the channel does not affect the streaming potential along the centerline of the tube in the first order of δ.

In order to investigate the effect of curvature on the streaming potential field, it is necessary to solve the second-order problem (54). Substituting Eqs. (31), (41), (45), and the expression of $V_1(r)$ into Eq. (54), we shall finally get the second-order streaming potential as

$$E_{\mathrm{s},2} = \frac{D_1}{u_r(2\varphi^2 T_{2,2} - M)}, \tag{56}$$

where the detailed expressions for D_1 and $T_{2,2}$ are sophisticated and not given here.

4 Results and discussion

The asymptotic solutions of the EDL potential, streaming potential, and the axial velocity have been derived up to $O(\delta^2)$. The involved dimensionless parameters include the inverse of the dimensionless Debye length k, the wall zeta potential φ, the characteristic velocity ratio u_r, the curvature ratio δ, and the parameter M (equivalent to the ionic Peclet number). To extend the analysis, calculations have been performed over wide ranges: M is set to change from 0.01 to 100, and k is from 1 to 100. In addition, we have taken the dimensionless wall zeta potential $\varphi = 1$ (i.e., $\widetilde{\varphi} = k_{\mathrm{B}}T/(ez_{\mathrm{v}}) = 26$ mV) and the parameter $u_r = 1$. The latter indicates the strength of comparable pressure-driven velocity and electroosmotic velocity.

4.1 First- and second-order EDL potential profiles

Figure 2 shows the three-dimensional (3D) profiles and contours of dimensionless first-order EDL potential distributions over the circular cross section of the channel for different k. Note that for plotting, we have transformed the polar coordinates (r, θ) in the cross section into the rectangular coordinates (X, Y) by

$$r = \sqrt{X^2 + Y^2}, \quad \theta = \arctan\frac{Y}{X}. \tag{57}$$

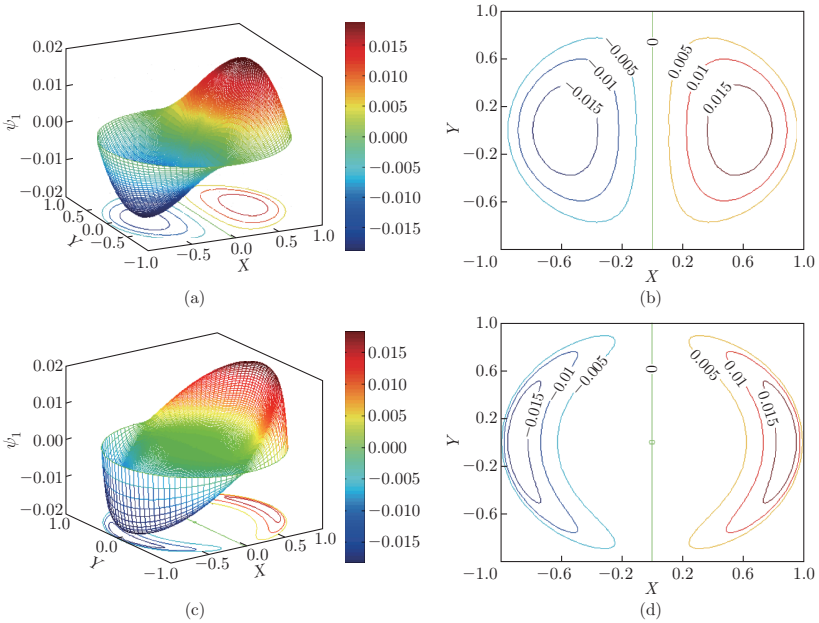

Fig. 2 3D distributions and contours of the first-order EDL potential, where (a) and (b) $k = 1$; (c) and (d) $k = 10$ (color online)

From Fig. 2, it can be observed that ψ_1 is anti-symmetric about the center of the cross section, as expected from Eq. (34). It is noteworthy that the effect of the first-order curvature tends to increase the EDL potential at the outer side of the bend (i.e., $-\pi/2 < \theta < \pi/2$) while to decrease the EDL potential at the inner side of the bend (i.e., $\pi/2 < \theta < 3\pi/2$). This leads to a skewed pattern in the overall EDL potential distribution, and a corresponding increase (decrease) in the amplitude of the normalized net charge density ρ_e by Eq. (22) at the outer (inner) side of the bend. Comparing Figs. 2(a) with 2(c), one can see that as k increases, the potential variations are restricted to a very narrow region close to the outer and inner walls. This can be explained by the fact that a large k means a thin EDL thickness.

The maximum of ψ_1 on the cross section of the channel, denoted by $\|\psi_1\|_\infty$, as a function of k is presented in Fig. 3. We found that $\|\psi_1\|_\infty$ reaches the maximum value 0.046 at about $k = 3$, which is 4.6% of the maximum value of ψ_0 ($\|\psi_0\|_\infty = \varphi = 1$). In addition, as $k \to \infty$, ψ_1 tends to zero.

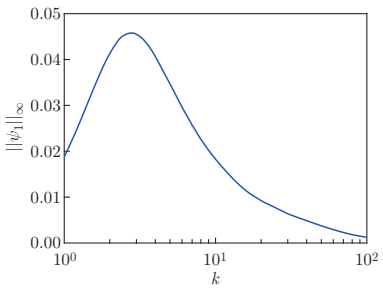

Fig. 3 Maximum of ψ_1 on the cross section of the channel as a function of k (color online)

Figure 4 depicts the 3D distributions and contours of dimensionless second-order EDL potential over the circular cross section of the channel for different k. It can be found that ψ_2 is symmetric about the center of the cross section. For all values of k, ψ_2 is of opposite sign to

ψ_0, indicating that the order δ^2 impact of the channel curvature is a reduction of the overall EDL potential at the whole cross section, and $\|\psi_2\|_\infty$, denoting the maximum of $|\psi_2|$, reaches its maximum value 0.032 at about $k = 3$ again (the figure is not shown here).

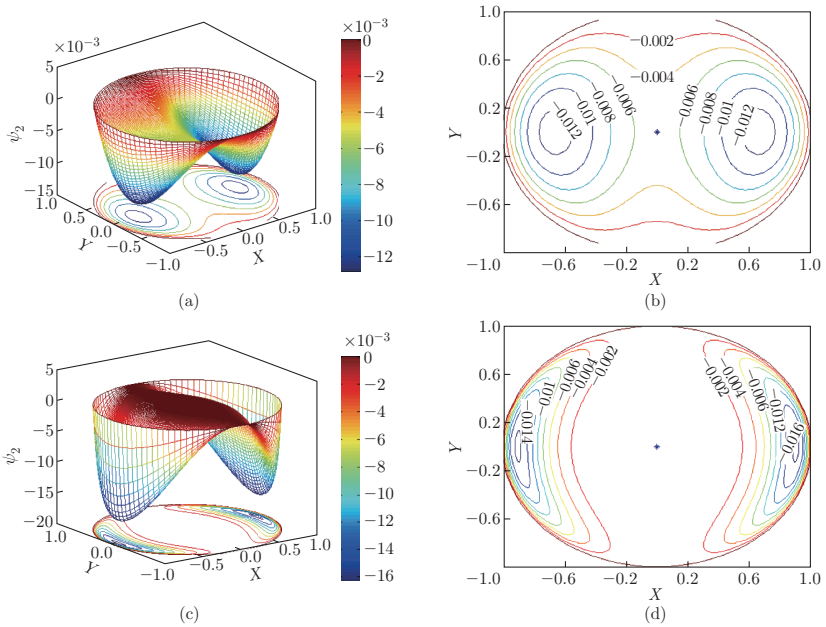

Fig. 4 3D distributions and contours of the second-order EDL potential, where (a) and (b) $k = 1$; (c) and (d) $k = 10$ (color online)

4.2 Streaming potential distribution

In the curvilinear coordinate system, the streaming potential field induced by the pressure-driven transport can be expressed as

$$\widetilde{\boldsymbol{E}}_{\mathrm{s}} = -\nabla\widetilde{\psi}_{\mathrm{s}} = \left(0,\ 0,\ -\frac{1}{R + r\cos\theta}\frac{\mathrm{d}\widetilde{\psi}_{\mathrm{s}}}{\mathrm{d}\phi}\right)^{\mathrm{T}} = \left(0,\ 0,\ \frac{\widetilde{E}_{\mathrm{s}}}{1 + \delta r'\cos\theta}\right)^{\mathrm{T}}, \tag{58}$$

where $\widetilde{E}_{\mathrm{s}}$ is the magnitude of the streaming potential field along the central axis of the channel (i.e., $r = 0$), defined by Eq. (11). The asymptotic solution of the dimensionless streaming potential E_{s} has been derived until the order δ^2 in Subsection 3.2.

Effects of the dimensionless parameters k and M on the streaming potential are investigated in Fig. 5 (Note that $E_{\mathrm{s},1}$ is zero). In Fig. 5(a), $E_{\mathrm{s},0}$ corresponds to the streaming potential in straight channels, and its magnitude (i.e., $|E_{\mathrm{s},0}|$) will decrease as increase in M for any given k, which is attributed to the fact that the increase in M will enhance the conductive effects, thereby leading to a lower streaming potential in magnitude; see Ref. [25]. In addition, $|E_{\mathrm{s},0}|$ will drop to zero quickly with the increase of k. Such a behavior is in accord with the relatively thin EDL.

In Fig. 5(b), it can be observed that $E_{\mathrm{s},2}$ has a sign opposite to $E_{\mathrm{s},0}$, and they are similar in the way of the dependence on parameters (i.e., $E_{\mathrm{s},2}$ will drop to zero with the increase of k or M). Thus, the curvature of the channel has a reduced effect on the streaming potential.

4.3 Axial velocity profile

The governing equations for the axial flow are Eqs. (25), (27), and (29). The zeroth-order solution (31) agrees well with the result for the electrokinetic flow in a straight pipe (see Ref. [12] or [25]). Figure 6 plots u_0 as a function of r for different dimensionless parameters k and M. Note that for small M and moderate k (e.g., k from 5 to 20), the backflow in the EDL near the wall can be witnessed in Fig. 6(a), even though the backflow is small. As mentioned above,

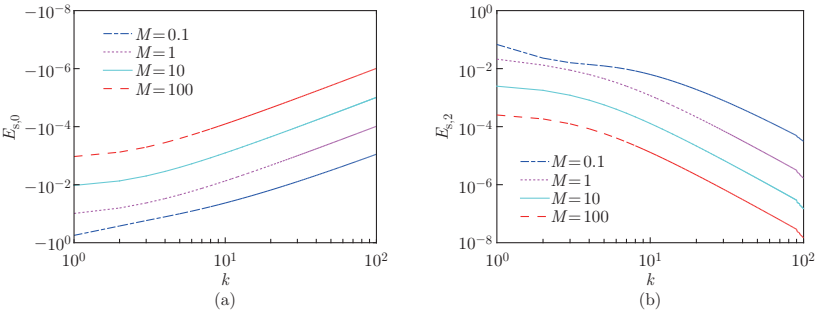

Fig. 5 Variations of the zeroth-order and second-order streaming potentials as a function of k for different values of M (color online)

the overall velocity profile is a superposition of the pressure-driven flow and the counteracting electroosmotic flow induced by streaming potential. For small M, the streaming potential field is so large (see Fig. 5(a)) that the contribution of pressure to the flow is not as great as the contribution of electroosmotic flow in the opposite direction caused by the migration of the ions in the EDL. This leads to the presence of the backflow near the walls.

With the increase in k or M, the streaming potential decreases rapidly in magnitude. As a result, the pressure-driven flow dominates the electroosmotic flow, the axial velocity increases and the backflow disappears completely. As expected, the axial velocity profile rises in a parabolic shape up to its maximum value 0.25 at the center of the channel (see Fig. 6), which is in accord with Eq. (31). Furthermore, as M continues to increase (e.g., $M = 10$), the effect of EDL on the velocity profile becomes negligible (see Fig. 6(d)).

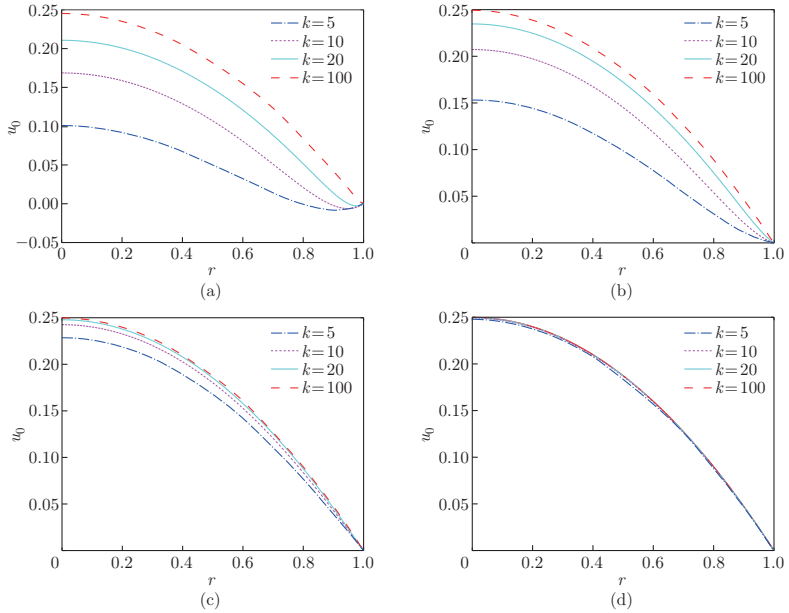

Fig. 6 Variations of the zeroth-order velocity distribution with dimensionless parameters k and M: (a) $M = 0.01$, (b) $M = 0.1$, (c) $M = 1$, and (d) $M = 10$ (color online)

The first-order velocity u_1 is given by Eq. (40). Because $E_{s,1}$ is zero, u_1 is anti-symmetric about the center. From Fig. 7(a), one can see that in the EDL, the first-order curvature has an opposite effect on the backflow. Outside the EDL, the effect of the first-order curvature tends to increase the axial velocity at the inner side of the bend while to decrease it at the outer side of the bend. This leads to an inward shift of the position of maximum velocity in the curved

channel. This is different from the behavior of inertial flows, where an outward shift in the maximum velocity occurs[6].

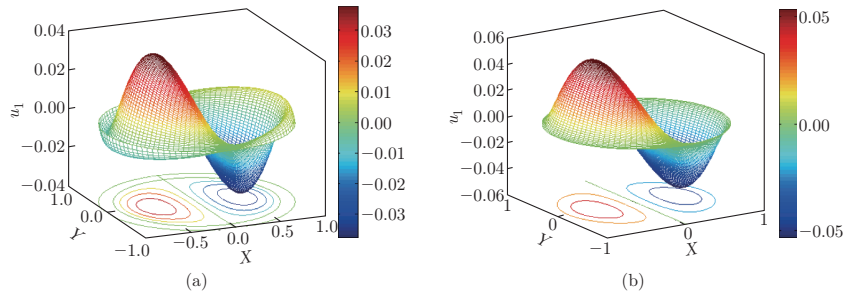

Fig. 7 3D first-order velocity distributions: (a) $k = 10$, $M = 0.01$; (b) $k = 10$, $M = 0.1$ (color online)

In general, the axial velocity redistribution is parameter dependent, and this behavior results from two competing effects induced by the channel curvature, i.e., the geometric and inertial effects[26]. For low Reynolds number flows, the geometric effect will play a major role, and the shift of maximum velocity is inward, while for high Reynolds number flows, the inertial effect dominates the geometric one, which leads to a significant secondary flow on the cross section and an outward shift in the maximum of the axial velocity.

In Fig. 8, we plot the variation of $\|u_1\|_\infty$, which is the maximum of $|u_1|$ on the cross section of the tube, with respect to k on a log scale at different M. This figure demonstrates that the reduction of velocity, caused by the presence of EDL, is remarkable when k is of the order of $O(1)$, especially for small M. The EDL effect disappears for the limiting case of $k \to \infty$, since $k \to \infty$ corresponds to an infinitely thin EDL. In this limiting case, the velocity u_1 tends to u_1^* in Eq. (43), where u_1^* reaches its extreme value ± 0.072 at about $r = 0.5774$ and $\theta = 0, \pi$. Thus, $\|u_1\|_\infty$ tends to 0.072 when $k \to \infty$, as illustrated in Fig. 8, which is up to 28.8% of the maximum value of u_0. Similar to the case of u_0, the effect of EDL on the first-order velocity also becomes negligible for large M.

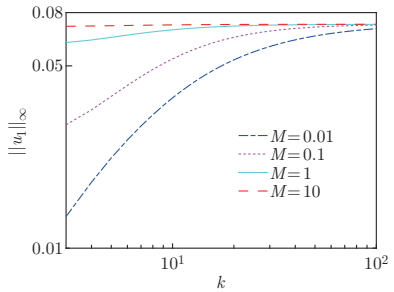

Fig. 8 Variations of $\|u_1\|_\infty$ with the dimensionless electrokinetic width k for different values of M (color online)

The profile of the second-order velocity u_2 is displayed in Fig. 9. The variations of u_2 with parameters k and M are similar to those of u_0 and u_1. For small M and moderate k, the influence of the EDL is significant, accompanied by the presence of backflow near the wall (see Fig. 9(a)). On the other hand, the EDL effect will disappear for the limiting case of $k \to \infty$. Under this circumstance, the velocity u_2 will tend to u_2^* in Eq. (47). The profile in Fig. 9(b) is typical, where the second-order curvature leads to an increase in the axial velocity at both the inner and outer side of the bend, but tends to reduce the velocity at the center of the tube. Moreover, the maximum value of u_2 is 0.03 from Eq. (47), which is 12% of the maximum value of u_0.

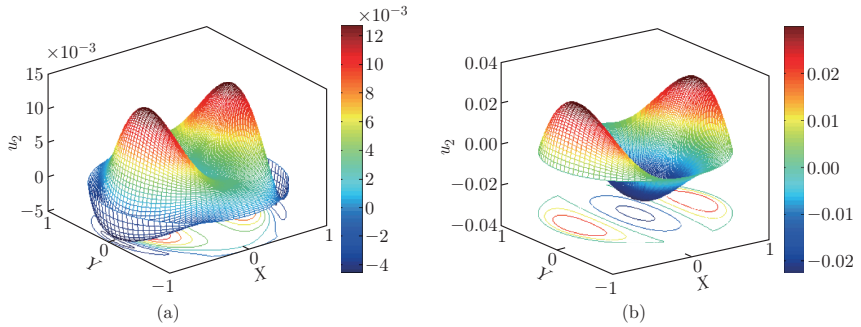

Fig. 9 3D distributions and contours for the second-order perturbation velocity, where (a) $k = 5$, $M = 0.01$, and (b) $k = 5$, $M = 10$ (color online)

4.4 Volume flow rate

The flow rate is a bulk property of the flow, and is given by integrating the asymptotic solution for the axial velocity over the channel cross section. Based on the velocity solutions (30), (40), and (44), we get the dimensionless flow rate as

$$Q = \int_0^{2\pi} \mathrm{d}\theta \int_0^1 u(r,\theta) r \,\mathrm{d}r = 2\pi \int_0^1 u_0(r) r \,\mathrm{d}r + 2\pi\delta^2 \int_0^1 u_2(r,\theta) r \,\mathrm{d}r = Q_0 + \delta^2 Q_2. \tag{59}$$

Here, Q_0 corresponds to the flow rate in a straight channel with the same cross section and with the same pressure gradient as the curved channel, and Q_2 represents an $O(\delta^2)$ effect of the curvature on the flow rate. Note that since $E_{\mathrm{s},1}$ vanishes and an integral of $\cos\theta$ over the cross section is also zero, the first-order perturbation velocity $u_1(r,\theta)$ in Eq. (40) makes no contribution to the flow rate. The expressions of Q_0 and Q_2 can be obtained as follows:

$$Q_0 = \frac{\pi}{8} + 2\pi\varphi u_r E_{\mathrm{s},0}\Big(\frac{1}{2} - \frac{\mathrm{I}_1(k)}{k\mathrm{I}_0(k)}\Big), \tag{60}$$

$$\begin{aligned} Q_2 = {} & \frac{\pi}{384} + 2\pi\varphi u_r E_{\mathrm{s},2}\Big(\frac{1}{2} - \frac{\mathrm{I}_1(k)}{k\mathrm{I}_0(k)}\Big) + 2\pi\varphi u_r E_{\mathrm{s},0}\Big(\Big(\frac{3}{2k^2} - B\Big)\Big(\frac{1}{2} - \frac{\mathrm{I}_1(k)}{k\mathrm{I}_0(k)}\Big) \\ & - \frac{k^2}{2}\sum_{n=1}^{\infty} \frac{b_{n,1}(2\mu_{n,1}^2 + k^2)}{\mu_{n,1}^3(\mu_{n,1}^2 + k^2)^2 \mathrm{J}_0(\mu_{n,1})} - \frac{k^2}{2}\sum_{n=1}^{\infty} \frac{b_{n,0}}{\mu_{n,0}^3(\mu_{n,1}^2 + k^2)\mathrm{J}_1(\mu_{n,0})} \\ & + \frac{2k^3\mathrm{I}_0(k) - 15k^2\mathrm{I}_1(k) + 32k\mathrm{I}_0(k) - 64\mathrm{I}_1(k)}{16k^3\mathrm{I}_0(k)}\Big), \end{aligned} \tag{61}$$

where $B = \sum\limits_{n=1}^{\infty} \frac{b_{n,1}\mu_{n,1}}{(\mu_{n,1}^2+k^2)^2\mathrm{J}_0(\mu_{n,1})}$, and $b_{n,v}$ is defined in Eq. (46).

Consider the limiting case of $k \to \infty$, i.e., an infinitely thin EDL. Using the estimates $\mathrm{I}_0(k) \approx \mathrm{I}_1(k)$, $E_{\mathrm{s},0} \sim O(k^{-2})$, and $E_{\mathrm{s},2} \sim O(k^{-2})$ with large k in Eqs. (60) and (61), we get

$$Q_0 \to \frac{\pi}{8}, \quad Q_2 \to \frac{\pi}{384} \quad \text{as} \quad k \to \infty, \tag{62}$$

which have been verified in Fig. 10. Furthermore, by using the above asymptotic limit, the ratio of the flow rate in a curved tube to the flow rate in a straight tube having the same cross section and the same pressure gradient reduces to $Q/Q_0 \approx 1 + \delta^2/48$, which is suitable for low Reynolds number flows.

Figure 10 illustrates the variations of the zeroth- and second-order normalized flow rates with k for different M. It can be found that the streaming potential causes a reduction in Q_0, as expected. The variation of Q_2 is complicated. In particular, there is a critical value $k_0 \approx 13$. When $k < k_0$, the streaming potential leads to the increase in Q_2; when $k > k_0$, it leads to the decrease in Q_2, compared with the limit value in Eq. (62). However, Q_2 is always positive in the ranges of k and M, which implies that the flow rate of electrokinetic flow in a curved

microtube is larger than that in a straight microtube having the same cross section and the same pressure gradient where the pressure gradient in the curved tube which is measured along the center circle of the curved tube. Figure 11 demonstrates the variations of the ratio of the flow rate in a curved tube to that in a straight tube with respect to the curvature ratio δ and M.

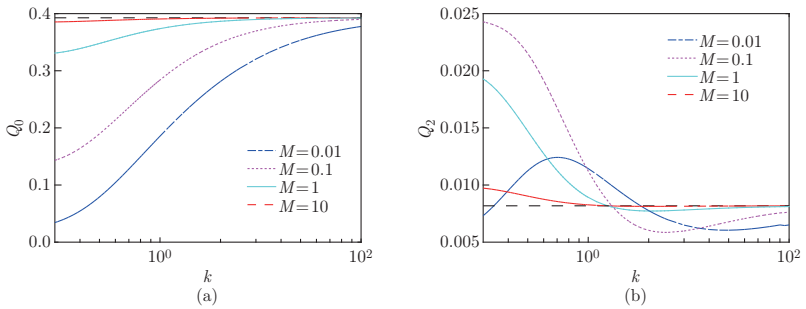

Fig. 10 Variations of the zeroth-order and second-order flow rates with dimensionless electrokinetic width k for different M, where the black dashed lines represent the values of flow rates without the electrokinetic effect, given by Eq. (62) (color online)

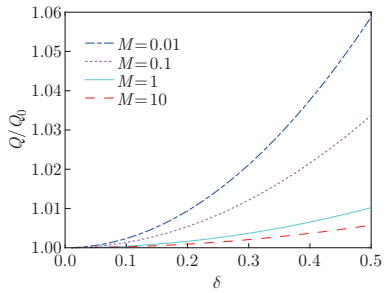

Fig. 11 Ratios of the flow rate of the curved microtube to the straight one as a function of δ for different values of M, with $k = 1$ (color online)

4.5 EKEC

When pressure-driven fluid flows through microchannels, the streaming current and streaming potential are generated. The streaming potential field can be used to drive an external load, and therefore represents a means of converting mechanical work into electrical power. The energy conversion efficiency needs to be considered for practical applications of such devices. Therefore, the research of EKEC efficiency in curved microchannels is valuable.

The EKEC efficiency is defined as

$$\eta = \frac{\widetilde{P}_{\text{out}}}{\widetilde{p}_{\text{in}}}, \tag{63}$$

where $\widetilde{P}_{\text{in}}$ and $\widetilde{P}_{\text{out}}$ are the input and output powers, respectively, expressed in the curved microtube by

$$\widetilde{p}_{\text{in}} = \int_0^{2\pi} \mathrm{d}\theta \int_0^a \Big(-\frac{1}{R + r\cos\theta} \frac{\partial \widetilde{p}}{\partial \phi} \Big) \widetilde{u}_p(r,\theta) r \,\mathrm{d}r, \tag{64}$$

$$\widetilde{p}_{\text{out}} = \frac{ez_{\text{v}}}{4} \int_0^{2\pi} \mathrm{d}\theta \int_0^a (n_+ + n_-) \frac{ez_{\text{v}}}{f} \Big(\frac{\widetilde{E}_{\text{s}} R}{R + r\cos\theta} \Big)^2 r \,\mathrm{d}r. \tag{65}$$

Note that in a curved microtube, the distributions of the pressure gradient and the streaming potential on the cross section of the tube are no longer uniform. In addition, the purely pressure-

driven fluid velocity, $\widetilde{u}_p$, is adopted in Eq. (64), which can be obtained by taking the streaming potential as zero in the expression of the velocity[20], i.e.,

$$\begin{cases} \widetilde{u}_p(r,\theta) = \Big(-\dfrac{a^2}{\mu R}\dfrac{\partial \widetilde{p}}{\partial \phi}\Big) u_p(r,\theta), \\ u_p(r,\theta) = \dfrac{1-r^2}{4} + \delta \dfrac{3r(r^2-1)}{16}\cos\theta + \delta^2\Big(\dfrac{14r^2-3-11r^4}{128} + \dfrac{5r^2(1-r^2)}{64}\cos 2\theta\Big). \end{cases} \tag{66}$$

Thus, using the dimensionless quantities in Eq. (17), we get the input and output powers as

$$\begin{aligned} \widetilde{p}_{\rm in} &= \Big(-\frac{a^2}{\mu R}\frac{\partial \widetilde{p}}{\partial \phi}\Big)\Big(-\frac{a^2}{R}\frac{\partial \widetilde{p}}{\partial \phi}\Big)\int_0^{2\pi} {\rm d}\theta \int_0^1 \frac{u_p(r,\theta)}{1+\delta r'\cos\theta} r'{\rm d}r' \\ &= \Big(-\frac{a^2}{R}\frac{\partial \widetilde{p}}{\partial \phi}\Big)^2 \frac{\pi}{\mu}\Big(\frac{1}{8} + \frac{5}{128}\delta^2 + o(\delta^2)\Big), \end{aligned} \tag{67}$$

$$\widetilde{p}_{\rm out} = \frac{Mk^2}{4\mu}\Big(-\frac{a^2}{R}\frac{\partial \widetilde{p}}{\partial \phi}\Big)^2 u_r^2 E_{\rm s,0} \times \Big(\pi E_{\rm s,0} + \delta^2\Big(\frac{3\pi}{4}E_{\rm s,0} + 2\pi E_{\rm s,2}\Big) + o(\delta^2)\Big). \tag{68}$$

It is noteworthy that the input and output powers are independent of δ to the first order. Substituting Eqs. (67) and (68) into Eq. (63), we finally get the EKEC efficiency as

$$\eta = \frac{8Mk^2u_r^2E_{\rm s,0}(4E_{\rm s,0} + \delta^2(3E_{\rm s,0} + 8E_{\rm s,2}) + o(\delta^2))}{16 + 5\delta^2 + o(\delta^2)}. \tag{69}$$

The variations of the EKEC efficiency with δ are presented in Fig. 12 for different values of k and M. From Fig. 12(a), it is observed that for the fixed $M = 0.01$, the efficiency increases as δ increases from zero. Furthermore, we find that the EKEC efficiency is around $1\% \sim 3\%$ in the limiting case of $\delta \to 0$. These values are in reasonable agreement with the previous experimental results in straight microchannels.

For large M, the efficiency becomes small and has a slight declining trend with δ for some values of k (see Fig. 12(b)). The effects of the parameters M and k on the EKEC efficiency can be explained by examining the variations of input and output powers. First, we notice that both the input and output powers are increased in the curved pipe with the increase in δ, but their growth rates are different, where the growth rate is defined by the ratio of the second-order term to the first-order term. The growth rate of input power is a constant 5/16 by Eq. (67), and the growth rate of output power is $3/4 + 2E_{\rm s,2}/E_{\rm s,0}$, whose variations are displayed in Fig. 13(a). When M is small, the growth rate of the output power is larger than that of the input power, leading to an increasing EKEC efficiency with δ. While for large M, the growth rate of the output power is lower than that of the input power within some range of k, resulting in a slight reduction in the EKEC efficiency with δ.

Furthermore, a critical curve can be defined in the parameter plane (k, M) by equating the

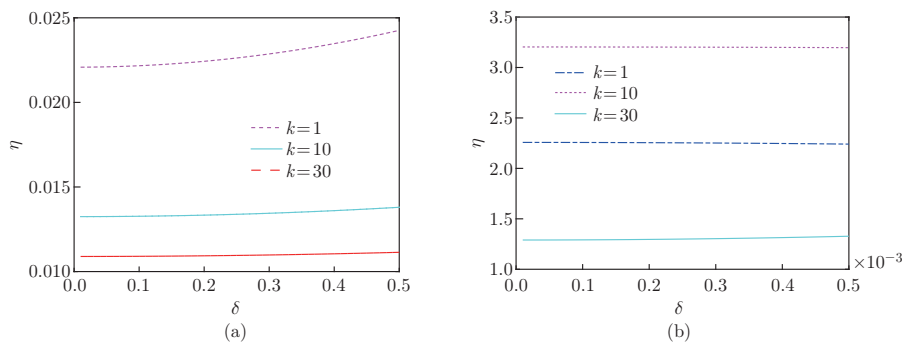

Fig. 12 Variations of the EKEC efficiency with δ for different k, where (a) $M = 0.01$ and (b) $M = 10$ (color online)

growth rate of output power with that of input power, and it is demonstrated in Fig. 13(b). If the point on the parameter plane is above the critical curve, the energy conversion efficiency will decrease with δ. Conversely, if the point on the parameter plane is below the critical curve, the energy conversion efficiency will increase with δ. In particular, it can be found that the maximum EKEC efficiency occurs at relatively small k and M in the parameter plane, where the curved-channel shape helps to improve the maximum EKEC efficiency.

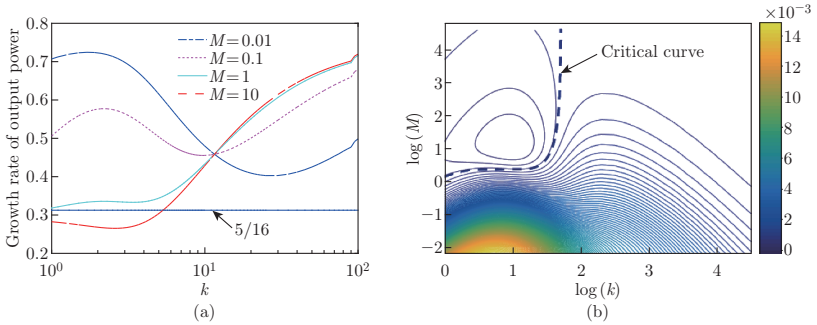

Fig. 13 (a) Variations of the growth rate of output power with k for different M, where the growth rate of input power (i.e., 5/16) is also shown for reference; (b) critical curve and contours of the EKEC efficiency in the parameter plane (k, M) with a double log scale and $\delta = 0.5$ (color online)

5 Conclusions

The effects of the curvature on the electrokinetic flow and energy conversion in a curved microtube are investigated by using a perturbation solution. The following conclusions are drawn. The curvature of the microtube leads to a skewed pattern in the EDL potential distribution. In a curved microtube, the EDL potential at the outer side of the bend is larger than that at the inner side of the bend. The calculation of the streaming potential indicates that the curvature of the channel does not affect the streaming potential along the centerline of the tube to the first-order in δ. The second-order term $E_{s,2}$ has a sign opposite to the zeroth-order term $E_{s,0}$. Therefore, the curvature shows an inhibitory effect on the magnitude of the streaming potential field.

The electrokinetic transport in a curved microchannel shows a significant difference compared with that in a straight one. Firstly, an inward shift of the position of maximum velocity occurs in the curved channel. Secondly, the flow rate in a curved microtube could be larger than that in a straight one with the same pressure gradient and shape of cross section. The asymptotic solutions of the axial velocity and flow rate in the absence of electrokinetic effect are in agreement with the classical results for a low Reynolds number limit. Finally, it is interesting to find that the curved-channel shape could be beneficial to improving the maximum EKEC efficiency based on the parameter study.

References

[1] CHEN, L., YANG, C., XIAO, Y., YAN, X., HU, L., EGGERSDORFER, M., CHEN, D., WEITZ, D. A., and YE, F. Milli-, micro- and nano-fluidics: manipulating fluids at varying length scales. *Materials Today Nano*, **16**, 100136 (2021)

[2] LASER, D. J. and SANTIAGO, J. G. A review of micropumps. *Journal of Micromechanics and Microengineering*, **14**, R35–R64 (2004)

[3] STONE, H. A., STROOCK, A. D., and AJDARI, A. Engineering flows in small devices: microfluidics toward a lab-on a-chip. *Annual Review of Fluid Mechanics*, **36**, 381–411 (2004)

[4] CHO, C. C., CHEN, C. L., and CHEN, C. K. Mixing of non-Newtonian fluids in wavy serpentine microchannel using electrokinetically driven flow. *Electrophoresis*, **33**, 743–750 (2012)

[5] OKAFOR, O., WEILHARD, A., FERNANDES, J. A., KARJALAINEN, E., GOODRIDGE, R., and SANS, V. Advanced reactor engineering with 3D printing for the continuous-flow synthesis of silver nanoparticles. *Reaction Chemistry & Engineering*, **2**, 129–136 (2017)

[6] BERGER, S. A., TALBOT, L., and YAO, L. S. Flow in curved pipes. *Annual Review of Fluid Mechanics*, **15**, 461–512 (1983)

[7] VASHISTH, S., KUMAR, V., and NIGAM, K. A review on the potential applications of curved geometries in process industry. *Industrial & Engineering Chemistry*, **47**, 3291–3337 (2008)

[8] DEAN, W, R. Note on the motion of fluid in a curved pipe. *Philosophical Magazine*, **4**, 208–223 (1927)

[9] DEAN, W. R. Fluid motion in a curved channel. *Philosophical Magazine*, **5**, 673–695 (1928)

[10] HO, C. M. and TAI, Y. C. Micro-electro-mechanical-systems (MEMS) and fluid flows. *Annual Review of Fluid Mechanics*, **30**, 579–612 (1998)

[11] JIAN, Y., LIU, Q., and YANG, L. AC electroosmotic flow of generalized Maxwell fluids in a rectangular microchannel. *Journal of Non-Newtonian Fluid Mechanics*, **166**, 1304–1314 (2011)

[12] LYKLEMA J. *Fundamentals of Interface and Colloid Science*, Volume 2, Academic Press, New York (1995)

[13] XUAN, X. and LI, D. Thermodynamic analysis of electrokinetic energy conversion. *Journal of Power Sources*, **156**, 677–684 (2006)

[14] GOSWAMI, P. and CHAKRABORTY, S. Energy transfer through streaming effects in time-periodic pressure-driven nanochannel flows with interfacial slip. *Langmuir*, **26**, 581–590 (2010)

[15] YANG, J., LU, F., KOSTIUK, L. W., and KWOK, D. Y. Electrokinetic microchannel battery by means of electrokinetic and microfluidic phenomena. *Journal of Micromechanics and Microengineering*, **13**, 963–970 (2003)

[16] DAIGUJI, H., YANG, P., SZERI, A. J., and MAJUMDAR, A. Electrochemomechanical energy conversion in nanofluidic channels. *Nano Letters*, **4**, 2315–2321 (2004)

[17] NGUYEN, T., XIE, Y., DE VREEDE, L. J., VAN DEN BERG, A., and EIJKEL, J. C. T. Highly enhanced energy conversion from the streaming current by polymer addition. *Lab on a Chip*, **13**, 3210–3216 (2013)

[18] KILSGAARD, B., HALDRUP, S., CATALANO, J., and BENTIEN, A. High figure of merit for electrokinetic energy conversion in Nafion membranes. *Journal of Power Sources*, **247**, 235–242 (2014)

[19] DING, Z., JIAN, Y., and TAN, W. Electrokinetic energy conversion of two-layer fluids through nanofluidic channels. *Journal of Fluid Mechanics*, **863**, 1062–1090 (2019)

[20] DING, Z. and JIAN, Y. Electrokinetic oscillatory flow and energy conversion of viscoelastic fluids in microchannels: a linear analysis. *Journal of Fluid Mechanics*, **919**, A20 (2021)

[21] LUO, W. J. Transient electroosmotic flow induced by DC or AC electric fields in a curved microtube. *Journal of Colloid and Interface Science*, **278**, 497–507 (2004)

[22] YUN, J. H., CHUN, M. S., and JUNG, H. W. The geometry effect on steady electrokinetic flows in curved rectangular microchannels. *Physics of Fluids*, **22**, 052004 (2010)

[23] YAMAGUCHI, Y., TAKAGI, F., YAMASHITA, K., NAKAMURA, H., MAEDA, H., SOTOWA, K., ET AL. 3-D simulation and visualization of laminar flow in a microchannel with hair-pin curves. *AIChE Journal*, **50**, 1530–1535 (2004)

[24] CHAKRABORTY, S. and DAS, S. Streaming-field-induced convective transport and its influence on the electro viscous effects in narrow fluidic confinement beyond the Debye-Hückel limit. *Physical Review E*, **77**, 037303 (2008)

[25] DAS, S., GUHA, A., and MITRA, S. K. Exploring new scaling regimes for streaming potential and electroviscous effects in a nanocapillary with overlapping electric double layers. *Analytica Chimica Acta*, **804**, 159–166 (2013)

[26] PICARDO, J. R. and PUSHPAVANAM, S. Core-annular two-phase flow in a gently curved circular channel. *AIChE Journal*, **59**, 4871–4886 (2013)